Real-time element position tracking of flexible array transducer for ultrasound beamforming

D. China, Z. Feng, H. Hooshangnejad, D. Sforza, P. Vagdargi, et al.

D. China, Z. Feng, H. Hooshangnejad, D. Sforza, P. Vagdargi, M. A. L. Bell, A. Uneri, K. Ding, "Real-time element position tracking of flexible array transducer for ultrasound beamforming," Proc. SPIE 12470, Medical Imaging 2023: Ultrasonic Imaging and Tomography, 124700A (10 April 2023); doi: 10.1117/12.2654435

SPIE.

Event: SPIE Medical Imaging, 2023, San Diego, California, United States

Real-time Element Position Tracking of Flexible Array Transducer for Ultrasound Beamforming

D. China,[a] Z. Feng,[b,c] H. Hooshangnejad,[a,b] D. Sforza,[b] P. Vagdargi,[a] M. A. L. Bell,[a,c] A. Uneri,[a] K. Ding *[b]

[a] Department of Biomedical Engineering, Johns Hopkins School of Medicine, Baltimore, MD, USA
[b] Department of Radiation Oncology and Molecular Radiation Sciences, Johns Hopkins School of Medicine, Baltimore, MD, USA
[c] Department of Electrical and Computer Engineering, Johns Hopkins University, Baltimore, MD, USA

ABSTRACT

Unlike traditional ultrasound (US) transducers with rigid casing, flexible array transducers can be deformed to patient-specific geometries, thus potentially removing user dependence during real-time monitoring in radiotherapy. Proper transducer geometry estimation is required for the transducer's delay-and-sum (DAS) beamforming algorithm to reconstruct B-mode US images. The main contribution of this work is to track each element's position of the transducer to improve the quality of reconstructed images. An NDI Polaris Spectra infrared tracker was used to localize the custom design optical markers and interfaced using the Plus toolkit to estimate the transducer geometry in real-time. Each marker was localized with respect to a reference marker. Each element's coordinate position and azimuth angle were estimated using a polygon fitting algorithm. Finally, DAS was used to reconstruct the US image from radio-frequency channel data. Various transducer curvatures were emulated using gel padding placed on a CIRS phantom. The geometric accuracy of localizing the optical markers attached to the transducer surface was evaluated using 3D Cone-Beam Computed Tomography (CBCT). The tracked element positions' deviations compared to the CBCT images were measured to be 0.50±0.29 mm. The Dice score for the segmented target structure from reconstructed US images was 95.1±3.3% for above mentioned error in element position. We have obtained a high accuracy (<1mm error) when tracking the element positions with different random curvatures. The proposed method can be used for reconstructing US images to assist in real-time monitoring of radiotherapy, with minimal user dependence.

Keywords: Flexible array transducer, ultrasound imaging, ultrasound beamforming, surface geometry estimation, image-guided radiotherapy

1. INTRODUCTION AND PURPOSE

Ultrasound (US) imaging in biomedical applications such as image-guided radiotherapy (IGRT) has increased in the last decade because of its non-ionizing nature and real-time imaging capability[1–13]. The use of other imaging modalities has been more common[14–24] than the use of US-based techniques in clinical applications of IGRT due to the rigid architecture of traditional US probe transducers. Pressure is often applied to improve acoustic contact, resulting in changes to anatomical structures during IGRT[25,26]. The flexible array transducer[27] has been employed to resolve the above-mentioned limitations. Due to the flexible nature of this probe, it can fit any surface geometry[28,29]. The flexible transducer's element position plays a vital role in B-mode US image reconstruction from radio-frequency (RF) channel data. Delay-and-sum (DAS) beamforming algorithm is required on RF channel data for the reconstruction of the image. An accurate element position has been required for a proper delay in each channel. The wrong delay can cause distortion and defocus on reconstructed US image.

The probe was first utilized for non-medical purposes, such as inspecting sub-surface defects and performing non-destructive testing (NDT)[30], etc. Several studies were carried out to reconstruct ultrasound images from the flexible probe by implementing appropriate delays. Casula et al. created a mechanical apparatus that automatically pushes transducer elements to the surface to estimate element positions[31]. Hunter et al. suggested an algorithm based on image sharpness optimization for generating ultrasound images[32]. Nakahata et al. proposed an offline method of generating ultrasound images by merging RF data and element position geometry during post-processing[33]. All of these methods were developed

Medical Imaging 2023: Ultrasonic Imaging and Tomography, edited by
Christian Boehm, Nick Bottenus, Proc. of SPIE Vol. 12470, 124700A

for non-biomedical tasks, and none of them were real-time approaches. Noda et al., Chang et al., and Omidvar et al. have suggested algorithms aimed at reconstructing precise biomedical US images. These algorithms utilize various optimization techniques such as entropy, variance, and gradient to achieve accurate US imaging results[34–36]. Real-time imaging can be challenging due to the iterative nature of these algorithms.

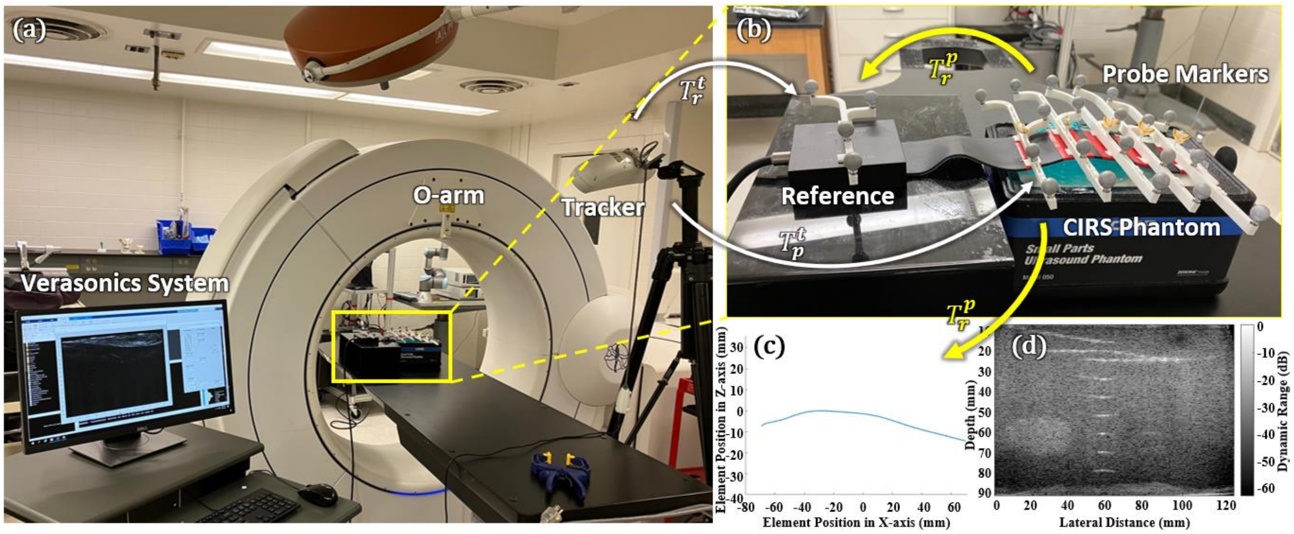

Figure 1. Experimental flow diagram (a) experimental setup where Verasonics system was used as a workstation, O-arm has been used to acquire CBCT from comparison and on the other side tracker was used to track the markers, (b) placement of the markers.

In order to achieve real-time US image reconstruction, researchers have explored deep neural network (DNN) based methods. Nair et al. utilized a DNN approach to replace the conventional beamforming step by processing the channel data to produce segmented targets and US images simultaneously[37,38]. The training of the network was conducted using a simulated dataset, where it was assumed that the element positions were linear. Simson et al., Yoon et al., Khan et al., and Luijten et al. presented end-to-end DNN-based approaches to produce high-quality B-mode US images from complete or subsampled RF data[39–42]. However, these methods utilized either time-delayed channel data or rigid probe geometry in beamforming, which is an impractical scenario for clinical applications. Huang et al. introduced a DNN-based US beamforming technique that enables direct formation of images from acquired RF data without the requirement of knowledge of flexible probe shape geometry[43]. Although the algorithm is capable of real-time US image reconstruction, its accuracy may decrease when presented with unseen geometries as it is a data-driven approach that is trained on simulated data. As a result, the usability of the above DNN-based methods in clinical applications may be limited. Indeed, it is crucial to develop an approach that can address the challenges of real-time US image reconstruction while maintaining high accuracy and reliability for a wide range of geometries encountered in clinical applications.

Optical trackers have been significant in image-guided surgery and IGRT over past two decades[44–47]. Due to their highly precise capabilities, optical trackers can be utilized to accurately estimate the geometry of flexible transducers in real-time. A novel method and experimental setup called the Flexible Transducer with External Tracking (FLEX) system has been proposed here to accurately extract all element positions from any transducer geometry or curvature. This experimental setup aims to achieve two goals: (1) acquire accurate US images of patient-specific geometries, and (2) remove user dependence during real-time monitoring in radiotherapy. Figure 1 shows the experimental setup for real-time US image reconstruction.

2. METHODS

The main contributions of this research are: 1) the development of a custom optical marker design that can be placed on the precise location of a flexible transducer element so that they can be tracked by optical tracker, 2) the estimation of element positions by analyzing the transformation tree of the tracked markers, and 3) the reconstruction of ultrasound images using the acquired RF data and the tracked element positions of the flexible array transducer.

2.1 Marker specifications

A total of five probe markers and one reference marker were used for the experiment. The probe markers placed on the {1st, 33rd, 65th, 97th, and 128th} elements of the probe transducer as shown in Figure 1(b). To avoid interference between markers, specially designed optical markers were created following Northern Digital Inc. (NDI) marker design protocols. The centroid of each marker was estimated using a stylus. The NDI Polaris Spectra infrared camera was used to track both the markers and stylus, while real-time hardware communications were handled through the Plus toolkit[48].

2.2 Element position estimation

The optical tracker is capable of tracking both reference markers (r) and probe markers (p) in real-time and estimate transformations T_r^t and T_p^t, respectively. These transformations have been utilized to determine the transformation T_r^p of the reference marker with respect to the probe marker.

$$T_r^p = (T_p^t)^{-1} T_r^t \tag{1}$$

where T_p^t and T_r^t are the transformation of the probe marker and reference marker, respectively, with respect to the tracker (t). The centroid of the markers was calculated using a stylus (s).

$$T_s^p = (T_p^t)^{-1} T_s^t \tag{2}$$

where T_s^p and T_s^t are the stylus pose with respect to the p and t, respectively.

The transformation matrices T_r^p obtained from all probe markers were used to determine the coordinates of the corresponding transducer elements. The flexible transducer's geometry was estimated using a polygon curve fitting algorithm based on the coordinates of the five associated transducer elements. The azimuth angles between two consecutive transducer elements were estimated using equation (3), with the X-axis and Z-axis directions utilized in the calculation, while the Y-axis remained fixed, as there is no movement in that direction.

$$\theta_{n+1} = tan^{-1}(z_{n+1} - z_n / x_{n+1} - x_n) \tag{3}$$

where azimuth angle for $n + 1^{th}$ element has been denoted by θ_{n+1} and x_{n+1}, z_{n+1} are the coordinates in X- and Z-directions.

2.3 US beamforming with updated element position

The DAS beamformer is the conventional method for reconstructing the B-mode US images from RF data. This method requires accurate transducer element positions to calculate the time-of-flight (ToF) between each element and the focal point. The time delay is determined from the ToF, which has been applied to each RF channel data to generate a proper B-mode US image. The transducer's element position has been estimated accurately using the proposed method in real-time. The estimated element positions from the proposed method are used to update the old transducer element positions in the ToF calculation.

2.4 Probe, phantom, and system specifications

The CIRS (Model 050) small-parts ultrasound phantom has been employed to evaluate the proposed method. To generate random curvature shapes, a US gel pad was placed on top of the phantom, as shown in Figure 1(b). The flexible array transducer utilized in this study was manufactured by Hitachi and Japan Probe. The Vantage 128 system, made by Verasonics Inc., USA, has been employed to acquire the RF data and generate B-mode US images. Quantitative evaluation of the proposed method has been done using element position extracted using Cone-beam computed tomography (CBCT) done by Medtronic O-arm (Medtronics Inc., Minneapolis, MN). The self-adhesive radiographic marker's (CT- SPOT 119; Beekley Medical) position was extracted from the CBCT images, which were placed on the centroid of each probe marker. The transducer element position was reconstructed using the extracted marker position, which was then used for comparison.

3. RESULTS

The CIRS phantom was used to evaluate the proposed method in several ways, including 1) assessing the impact of incorrect element positioning in US beamforming and 2) examining the accuracy of FLEX in comparison to a CBCT-based element positioning estimation system.

3.1 Effect of the erroneous element position on US beamforming

This experiment was conducted to confirm the impact of incorrect element placement on US image reconstruction. The RF data was acquired using a linear probe geometry, and the resulting US image (Figure 2(a)) was used as the reference image for the experiment. Subsequently, the transducer's element position was randomly altered within the range of {0-1, 1-2, 2-3, …, 9-10}mm, and the corresponding reconstructed images were shown in Figure 2(b)-(i). To assess the structural distortion caused by the incorrect element position in US image reconstruction, the targets enclosed by the yellow border in each image of Figure 2 were segmented using a semi-automated threshold-based technique. The Dice-score was calculated for each segmented target relative to the reference image target and presented in Figure 3(b).

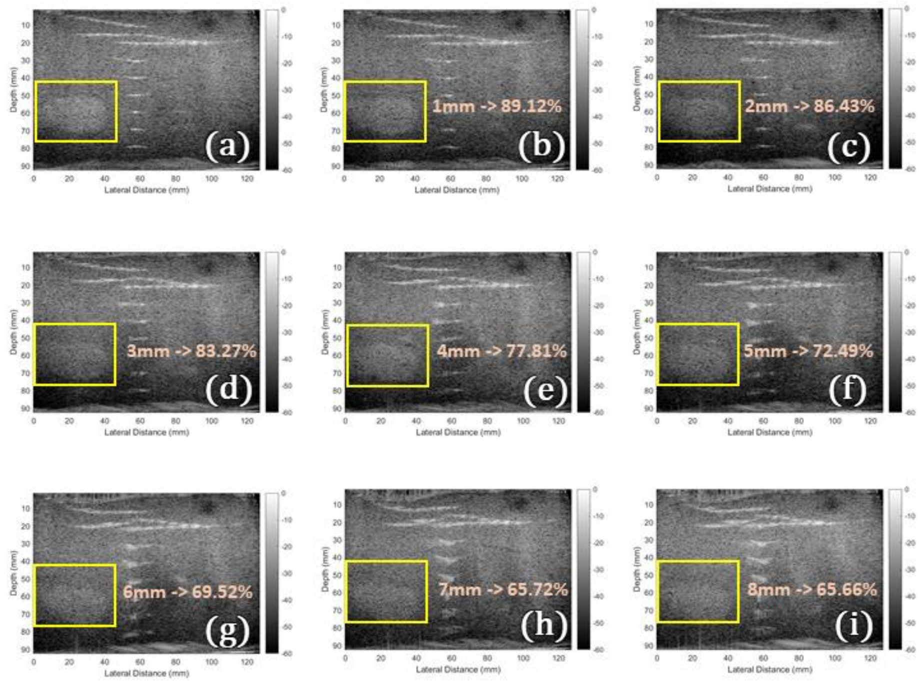

Figure 2. (a) reference image, which is generated and acquired by the linear position of flexible probe element position. (b)-(i) are the generated US images using the reference RF data with modified some of the element positions from 1-8mm, respectively. The yellow box visualizes the location of the phantom target changes, and the Dice-score with respect to the reference was mentioned on individual images.

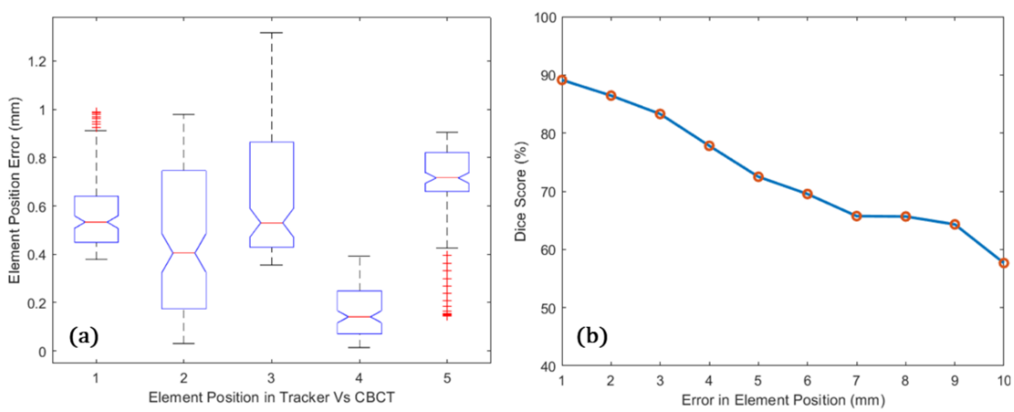

Figure 3. (a) element position error (distance between tracker Vs. CBCT) for different curvatures (X-axis labels belong to different curvatures). (b) deformation of the target structure (Dice score) compared with reference for the different range of error in element position (mm).

3.2 Accuracy of the FLEX-based element position tracking

In this experiment, the optical tracker's error was evaluated and estimated. To accomplish this, a reference (CBCT-based) system was employed. Self-adhesive radiographic markers (CT-spot) were placed on each marker's centroid, enabling identification in the CBCT volumes and estimation of the coordinate position of each marker. By comparing the position of each transducer element extracted from the FLEX and reference system, the tracker's error was estimated. To assess the error rate, five random curvatures were used, including linear, curvilinear, and arbitrary shapes. The deviation of the element positions was visualized using a boxplot, as shown in Figure 3(a), where the X-axis represents different probe shapes, and the Y-axis represents the deviation of the element positions. Overall 0.50±0.29 mm element position error has been obtained from this experiment. Additionally, we achieved a Dice score of 95.1±3.3% for this element position error.

4. DISCUSSION

4.1 Effect of the erroneous element position

US beamforming with erroneous element position cost to the structural deformation of the imaging target, as illustrated in Figure 2. In this figure, it is visually observed that the target structure deformation increased with the increase of the element position error rate. The quantitative evaluation has been done in this experiment by calculating the dice score of the segmented structure concerning the reference image segmented target. The target structure deformation rate in terms of the dice score is shown in Figure 3(b). The results of this experiment suggest that precise estimation of the element position is crucial for the reconstruction of accurate B-mode US images.

4.2 Accuracy of the proposed FLEX system

Section 4.1 indicates that in the case of flexible probes, the estimation of element position should be incorporated into the US image generation process. To resolve this issue, we proposed a system design (FLEX) based on some hardware, such as an optical tracker, custom design marker, etc., to estimate the accurate transducer array geometry. The precision of the suggested approach was evaluated with respect to a CBCT-based element position tracking system, as described in the preceding section. The deviation in the estimated position of a transducer element between the CBCT and FLEX-based solution was utilized as the error for the proposed system. This error was calculated for various curvatures and depicted in Figure 3(a). The figure indicates that the error rate of the proposed system is below 1 mm for different curvatures of the probe geometry. The experiment also reported an accuracy rate in terms of the Dice score, which was found to be 95.1±3.3% for an overall element position estimation error of 0.50±0.29 mm. These results demonstrate that the reconstructed US image closely resembles the actual US image, and the target structure remains consistent with the actual structure.

5. CONCLUSIONS

This study introduces a new FLEX system that tracks the position of flexible array transducer elements to reconstruct ultrasound (US) images. The experimental setup and results demonstrate that the tracked element coordinates are comparable to the ground truth. The dice score indicates that the resulting images with tracked element positions closely resemble the reference images. This research has the potential to facilitate the use of flexible probes for collecting US data from patients with various anatomies and to enable real-time monitoring during IGRT without the need for user input. In the next phase of evaluation, the system will be tested on clinically relevant data (e.g., from patients or cadavers) or a deformable phantom.

ACKNOWLEDGMENTS

This research was partly supported by the National Institutes of Health (award numbers R37CA229417 and T32AR067708). The content is solely the responsibility of the authors and does not necessarily represent the official views of the National Institutes of Health.

REFERENCES

[1] China, D., Illanes, A., Poudel, P., Friebe, M., Mitra, P. and Sheet, D., "Anatomical Structure Segmentation in Ultrasound Volumes Using Cross Frame Belief Propagating Iterative Random Walks," IEEE J Biomed Health Inform **23**(3) (2019).

[2] Feng, Z., Hooshangnejad, H., Shin, E. J., Narang, A., Lediju Bell, M. A. and Ding, K., "The Feasibility of Haar Feature-Based Endoscopic Ultrasound Probe Tracking for Implanting Hydrogel Spacer in Radiation Therapy for Pancreatic Cancer," Front Oncol **11** (2021).

[3] Kim, S., Ding, K., Rao, A., He, J., Bhutani, M. S., Herman, J. M., Narang, A. and Shin, E. J., "EUS-guided hydrogel microparticle injection in a cadaveric model," J Appl Clin Med Phys **22**(6), 83–91 (2021).

[4] Su, L., Iordachita, I., Zhang, Y., Lee, J., Ng, S. K., Jackson, J., Hooker, T., Wong, J., Herman, J. M., Sen, H. T., Kazanzides, P., Lediju Bell, M. A., Yang, C. and Ding, K., "Feasibility study of ultrasound imaging for stereotactic body radiation therapy with active breathing coordinator in pancreatic cancer," J Appl Clin Med Phys **18**(4), 84–96 (2017).

[5] Huang, P., Su, L., Chen, S., Cao, K., Song, Q., Kazanzides, P., Iordachita, I., Lediju Bell, M. A., Wong, J. W., Li, D. and Ding, K., "2D ultrasound imaging based intra-fraction respiratory motion tracking for abdominal radiation therapy using machine learning," Phys Med Biol **64**(18), 185006 (2019).

[6] Sen, H. T., Bell, M. A. L., Zhang, Y., Ding, K., Boctor, E., Wong, J., Iordachita, I. and Kazanzides, P., "System Integration and In Vivo Testing of a Robot for Ultrasound Guidance and Monitoring During Radiotherapy," IEEE Trans Biomed Eng **64**(7), 1608–1618 (2017).

[7] Şen, H. T., Cheng, A., Ding, K., Boctor, E., Wong, J., Iordachita, I. and Kazanzides, P., "Cooperative Control with Ultrasound Guidance for Radiation Therapy," Front Robot AI **3** (2016).

[8] Sen, H. T., Lediju Bell, M. A., Zhang, Y., Ding, K., Wong, J., Iordachita, I. and Kazanzides, P., "System integration and preliminary in-vivo experiments of a robot for ultrasound guidance and monitoring during radiotherapy," 2015 International Conference on Advanced Robotics (ICAR), 53–59, IEEE (2015).

[9] China, D., Mitra, P. and Sheet, D., [Segmentation of lumen and external elastic laminae in intravascular ultrasound images using ultrasonic backscattering physics initialized multiscale random walks] (2016).

[10] China, D., Nag, M. K., Mandana, K. M., Sadhu, A. K., Mitra, P. and Chakraborty, C., "Automated in vivo delineation of lumen wall using intravascular ultrasound imaging," Proceedings of the Annual International Conference of the IEEE Engineering in Medicine and Biology Society, EMBS **2016-Octob** (2016).

[11] China, D., Mitra, P. and Sheet, D., [On the fly segmentation of intravascular ultrasound images powered by learning of backscattering physics] (2018).

[12] China, D., Tom, F., Nandamuri, S., Kar, A., Srinivasan, M., Mitra, P. and Sheet, D., "Ultracompression: Framework for high density compression of ultrasound volumes using physics modeling deep neural networks," Proceedings - International Symposium on Biomedical Imaging **2019-April** (2019).

[13] Nandamuri, S., China, D., Mitra, P. and Sheet, D., "SUMNet: Fully convolutional model for fast segmentation of anatomical structures in ultrasound volumes," Proceedings - International Symposium on Biomedical Imaging **2019-April** (2019).

[14] Hooshangnejad, H. and Ding, K., "Feasibility of planning-CT-free rapid workflow for stereotactic body radiotherapy: removing the need for planning CT by AI-driven, intelligent prediction of body deformation," Medical Imaging 2022: Image-Guided Procedures, Robotic Interventions, and Modeling, C. A. Linte and J. H. Siewerdsen, Eds., 73, SPIE (2022).

[15] Hooshangnejad, H., Youssefian, S., Guest, J. K. and Ding, K., "*FEMOSSA*: Patient-specific finite element simulation of the prostate–rectum spacer placement, a predictive model for prostate cancer radiotherapy," Med Phys **48**(7), 3438–3452 (2021).

[16] Han, D., Hooshangnejad, H., Chen, C.-C. and Ding, K., "A Beam-Specific Optimization Target Volume for Stereotactic Proton Pencil Beam Scanning Therapy for Locally Advanced Pancreatic Cancer," Adv Radiat Oncol **6**(6), 100757 (2021).

[17] Rao, A. D., Shin, E. J., Meyer, J., Thompson, E. L., Fu, W., Hu, C., Fishman, E. K., Weiss, M., Wolfgang, C., Burkhart, R., He, J., Kerdsirichairat, T., Herman, J. M., Ding, K. and Narang, A., "Evaluation of a Novel Absorbable Radiopaque Hydrogel in Patients Undergoing Image Guided Radiation Therapy for Borderline Resectable and Locally Advanced Pancreatic Adenocarcinoma," Pract Radiat Oncol **10**(6), e508–e513 (2020).

[18] Kerdsirichairat, T., Narang, A. K., Thompson, E., Kim, S.-H., Rao, A., Ding, K. and Shin, E. J., "Feasibility of Using Hydrogel Spacers for Borderline-Resectable and Locally Advanced Pancreatic Tumors," Gastroenterology **157**(4), 933–935 (2019).

[19] Feng, Z., Rao, A. D., Cheng, Z., Shin, E. J., Moore, J., Su, L., Kim, S.-H., Wong, J., Narang, A., Herman, J. M., McNutt, T., Li, D. and Ding, K., "Dose Prediction Model for Duodenum Sparing With a Biodegradable Hydrogel

Spacer for Pancreatic Cancer Radiation Therapy," International Journal of Radiation Oncology*Biology*Physics **102**(3), 651–659 (2018).

[20] Rao, A. D., Shin, E. J., Beck, S. E., Garrett, C., Kim, S.-H., Lee, N. J., Liapi, E., Wong, J., Herman, J., Narang, A. and Ding, K., "Demonstration of Safety and Feasibility of Hydrogel Marking of the Pancreas–Duodenum Interface for Image Guided Radiation Therapy (IGRT) in a Porcine Model: Implications in IGRT for Pancreatic Cancer Patients," International Journal of Radiation Oncology*Biology*Physics **101**(3), 640–645 (2018).

[21] Rao, A. D., Coquia, S., de Jong, R., Gourin, C., Page, B., Latronico, D., Dah, S., Su, L., Clarke, S., Schultz, J., Rosati, L. M., Fakhry, C., Wong, J., DeWeese, T. L., Quon, H., Ding, K. and Kiess, A., "Effects of biodegradable hydrogel spacer injection on contralateral submandibular gland sparing in radiotherapy for head and neck cancers," Radiotherapy and Oncology **126**(1), 96–99 (2018).

[22] Rao, A. D., Feng, Z., Shin, E. J., He, J., Waters, K. M., Coquia, S., DeJong, R., Rosati, L. M., Su, L., Li, D., Jackson, J., Clark, S., Schultz, J., Hutchings, D., Kim, S.-H., Hruban, R. H., DeWeese, T. L., Wong, J., Narang, A., et al., "A Novel Absorbable Radiopaque Hydrogel Spacer to Separate the Head of the Pancreas and Duodenum in Radiation Therapy for Pancreatic Cancer," International Journal of Radiation Oncology*Biology*Physics **99**(5), 1111–1120 (2017).

[23] Han-Oh, S., Hill, C., Kang-Hsin Wang, K., Ding, K., Wright, J. L., Alcorn, S., Meyer, J., Herman, J. and Narang, A., "Geometric Reproducibility of Fiducial Markers and Efficacy of a Patient-Specific Margin Design Using Deep Inspiration Breath Hold for Stereotactic Body Radiation Therapy for Pancreatic Cancer," Adv Radiat Oncol **6**(2), 100655 (2021).

[24] Han-Oh, S., Ding, K., Song, D., Narang, A., Wong, J., Rong, Y. and Bliss, D., "Feasibility study of fiducial marker localization using microwave radar," Med Phys **48**(11), 7271–7282 (2021).

[25] Daft, C. M. W., "Conformable transducers for large-volume, operator-independent imaging," 2010 IEEE International Ultrasonics Symposium, 798–808, IEEE (2010).

[26] Bakerp, M., Juhler-Nøttrup, T. and Behrens, C. F., "Impact of Ultrasound Probe Pressure on Uterine Positional Displacement in Gynecologic Cancer Patients," Women's Health **10**(6), 583–590 (2014).

[27] Zhang, J., Wiacek, A., Gonzalez, E., Feng, Z., Ding, K. and Lediju Bell, M. A., "A Flexible Array Transducer for Photoacoustic-Guided Surgery," 2022 IEEE International Ultrasonics Symposium (IUS), 1–4, IEEE (2022).

[28] Casula, O., Poidevin, C., Cattiaux, G. and Fleury, G., "A FLEXIBLE PHASED ARRAY TRANSDUCER FOR CONTACT EXAMINATION OF COMPONENT WITH COMPLEX GEOMETRY," 2004.

[29] Yang, Y., Tian, H., Yan, B., Sun, H., Wu, C., Shu, Y., Wang, L.-G. and Ren, T.-L., "A flexible piezoelectric micromachined ultrasound transducer," RSC Adv **3**(47), 24900–24905 (2013).

[30] Lane, C. J. L., "The inspection of curved components using flexible ultrasonic arrays and shape sensing fibres," Case Studies in Nondestructive Testing and Evaluation **1**, 13–18 (2014).

[31] Casula, O., Toullelan, G., Roy, O. and Dumas, P., "ULTRASONIC NONDESTRUCTIVE TESTING OF COMPLEX COMPONENTS WITH FLEXIBLE PHASED-ARRAY TRANSDUCERS," 2010.

[32] Hunter, A. J., Drinkwater, B. W. and Wilcox, P. D., "Autofocusing ultrasonic imagery for non-destructive testing and evaluation of specimens with complicated geometries," NDT & E International **43**(2), 78–85 (2010).

[33] Nakahata, K., Tokumasu, S., Sakai, A., Iwata, Y., Ohira, K. and Ogura, Y., "Ultrasonic imaging using signal post-processing for a flexible array transducer," NDT & E International **82**, 13–25 (2016).

[34] Noda, T., Tomii, N., Nakagawa, K., Azuma, T. and Sakuma, I., "Shape Estimation Algorithm for Ultrasound Imaging by Flexible Array Transducer," IEEE Trans Ultrason Ferroelectr Freq Control **67**(11), 2345–2353 (2020).

[35] Chang, J., Chen, Z., Huang, Y., Li, Y., Zeng, X. and Lu, C., "Flexible ultrasonic array for breast-cancer diagnosis based on a self-shape–estimation algorithm," Ultrasonics **108**, 106199 (2020).

[36] Omidvar, A., Rohling, R., Cretu, E., Cresswell, M. and Hodgson, A. J., "An Intrinsic Shape Estimation Algorithm for Flexible Ultrasound Probes Intended for Clinical Applications," 2021 IEEE International Ultrasonics Symposium (IUS), 1–4, IEEE (2021).

[37] Nair, A. A., Tran, T. D., Reiter, A. and Lediju Bell, M. A., "A Deep Learning Based Alternative to Beamforming Ultrasound Images," 2018 IEEE International Conference on Acoustics, Speech and Signal Processing (ICASSP), 3359–3363, IEEE (2018).

[38] Nair, A. A., Washington, K. N., Tran, T. D., Reiter, A. and Lediju Bell, M. A., "Deep Learning to Obtain Simultaneous Image and Segmentation Outputs From a Single Input of Raw Ultrasound Channel Data," IEEE Trans Ultrason Ferroelectr Freq Control **67**(12), 2493–2509 (2020).

[39] Simson, W., Paschali, M., Navab, N. and Zahnd, G., "Deep Learning Beamforming for Sub-Sampled Ultrasound Data," 2018 IEEE International Ultrasonics Symposium (IUS), 1–4, IEEE (2018).

[40] Yoon, Y. H., Khan, S., Huh, J. and Ye, J. C., "Efficient B-Mode Ultrasound Image Reconstruction From Sub-Sampled RF Data Using Deep Learning," IEEE Trans Med Imaging **38**(2), 325–336 (2019).

[41] Khan, S., Huh, J. and Ye, J. C., "Adaptive and Compressive Beamforming Using Deep Learning for Medical Ultrasound," IEEE Trans Ultrason Ferroelectr Freq Control **67**(8), 1558–1572 (2020).

[42] Luijten, B., Cohen, R., de Bruijn, F. J., Schmeitz, H. A. W., Mischi, M., Eldar, Y. C. and van Sloun, R. J. G., "Adaptive ultrasound beamforming using deep learning," IEEE Trans Med Imaging **39**(12), 3967–3978 (2020).

[43] Huang, X., Lediju Bell, M. A. and Ding, K., "Deep Learning for Ultrasound Beamforming in Flexible Array Transducer," IEEE Trans Med Imaging **40**(11), 3178–3189 (2021).

[44] Tang, J., Dieterich, S. and Cleary, K. R., "Respiratory motion tracking of skin and liver in swine for Cyberknife motion compensation," 5 May 2004, 729.

[45] Spadea, M. F., Baroni, G., Riboldi, M., Tagaste, B., Garibaldi, C., Orecchia, R. and Pedotti, A., "Patient set-up verification by infrared optical localization and body surface sensing in breast radiation therapy," Radiotherapy and Oncology **79**(2), 170–178 (2006).

[46] Wilbert, J., Meyer, J., Baier, K., Guckenberger, M., Herrmann, C., Heß, R., Janka, C., Ma, L., Mersebach, T., Richter, A., Roth, M., Schilling, K. and Flentje, M., "Tumor tracking and motion compensation with an adaptive tumor tracking system (ATTS): System description and prototype testing," Med Phys **35**(9), 3911–3921 (2008).

[47] Desplanques, M., Tagaste, B., Fontana, G., Pella, A., Riboldi, M., Fattori, G., Donno, A., Baroni, G. and Orecchia, R., "A comparative study between the imaging system and the optical tracking system in proton therapy at CNAO," J Radiat Res **54**(suppl 1), i129–i135 (2013).

[48] Lasso, A., Heffter, T., Rankin, A., Pinter, C., Ungi, T. and Fichtinger, G., "PLUS: Open-Source Toolkit for Ultrasound-Guided Intervention Systems," IEEE Trans Biomed Eng **61**(10), 2527–2537 (2014).